Contents lists available at ScienceDirect

Applied Surface Science Advances

Pulsed laser deposition of thin films of TiO$_2$ for Li-ion batteries

Mariangela Curcio [a],[*], Angela De Bonis [a], Sergio Brutti [b],[c], Antonio Santagata [d], Roberto Teghil [a]

[a] *Dipartimento di Scienze, Università della Basilicata, V.le dell'AteneoLucano 10, 85100 Potenza, Italy*
[b] *Dipartimento di Chimica, Università di Roma La Sapienza, P.le Aldo Moro 5, 00185 Roma, Italy*
[c] *GISEL - Centro di Riferimento Nazionale per i Sistemi di Accumulo Elettrochimico di Energia, INSTM via G. Giusti 9, 50121 Firenze, Italy*
[d] *CNR-ISM, U.O.S.TitoScalo, Zona Industriale, 85050 TitoScalo, PZ, Italy*

ABSTRACT

Microbatteries produced by physical deposition methods are expected to play a pivotal role in many different micro-electronic applications such as stand-alone sensors, implantable or wearable medical devices, radio frequency identification-based systems and smart-cards. In this study pulsed laser deposition (PLD) using a femtosecond-pulsed laser has been applied to TiO$_2$ target materials to produce thin films of anatase-based nanoparticles on aluminum substrates suitable for application as negative electrode in Li-ion MBs. Different post-deposition treatments have been evaluated: films morphology and composition have been investigated with a multi-technique approach and the corresponding performance and electrochemical properties in Li-ion MBs have been analyzed by cyclic voltammetry and galvanostatic techniques. Compact and dense TiO$_2$ films composed by nanoparticles were obtained by PLD with co-crystallization of both anatase and rutile phases. Post-deposition annealing at temperature of 500 °C promote the rutile to anatase phase transition. As deposited TiO$_2$ films are electrochemically almost inactive in lithium half cells, whereas post deposition annealing (either in Ar or Air) boosts the electrochemical activity: air annealing outperforms Ar annealing. The additional deposition of a outer carbon layer by PLD on the TiO$_2$ films further improves the Li$^+$ transport properties, the reversibility of the electrochemical intercalation/de-intercalation reaction as well as the battery performance in terms of capacity retention upon cycling and rate response.

1. Introduction

The development of innovative portable electronic devices raises the question for reliable and scalable high-power density miniaturized energy storage devices, such as microbatteries (MBs). Stand-alone sensors, implantable or wearable medical devices, radio frequency identification (RFID)-based systems, smart cardsare examples of advanced technological systems requiring MBs with extended calendar life, high safety, large specificenergy and excellent power performance. Thin film electrodes produced by physical or chemical deposition techniques are the technological core of any MB. This approach has several advantages: easy design and manufacture, controllable electrode mass loading as well asuse of flexible electrode supports. Furthermore, thin film electrodes benefit of reduced transport paths of ions and electrons across all active battery components, thus leading to small internal cell resistances [1,2]. Aprotic Li-ion batteries (LIBs) are the most popular commercial energy storage devices for portable electronics: therefore, many studies proposed the re-shaping of this technology into MBs.

Among all the negative electrode materials demonstrated for LIBs the most common, graphite, suffers of several drawbacks that hinders its use

in MBs: (i) the precipitation of a solid electrolyte interface (SEI) during the first electrochemical lithium intercalation, with parallel release of gases, causing a remarkable mechanical stress on the electrode micromorphology and in the long term leading to capacity fading [3-5] and (ii) the formation of lithium dendrites at high current rates, that may lead to internal short circuiting and catastrophic cell failures. A number of other anode materials have been proposed for MBs, such as Li-metal alloys, silicon-, germanium- and tin-based materials, however, despite their greater capacities, the common problem arisen is their big volume expansion upon cycling [6,7]. In this context, nano-TiO$_2$ is a promising candidate as negative electrodes material for Li-ion MBs since it is characterized by good theoretical capacity (around 175 mAh/g), insertion potential in the range 1.5–1.9 V *vs.* Li$^+$/Li, small structural and volume change (~4%) during Li insertion/deinsertion, resulting safe and stable [7,8]. Moreover, TiO$_2$ is non-toxic, has low cost and its synthesis requires cheap and common raw materials.

The electrochemical lithium intercalation reaction of titanium oxide, i.e. $TiO_2 + xLi^+ + xe^- \rightleftarrows Li_xTiO_2 (0 \leq x \leq 0.5-0.9)$, involves the insertion/deinsertion of xLi^+ together with the Ti reduction/oxidation ($xTi(IV) \rightleftarrows xTi(III)$). This electrochemical reaction has been demonstrated

---

* Corresponding author.
E-mail address: mariangela.curcio@unibas.it (M. Curcio).

Table 1
Samples and post deposition treatments.

Sample coding	TO01	TO02	TO03	TO04
Carbon coating	None	None	None	PLD of graphite
Annealing at 500 °C	None	In Air, heating 10 °C min^{-1}, 2 h, natural cooling	Under Ar flow (80 ml min^{-1}), heating 10 °C min^{-1}, 2 h, natural cooling	

to be highly reversible for thousands of cycles. Various TiO$_2$ polymorphs have been investigated in LIBs, including anatase and rutile: among these, anatase shows superior electrochemical performances, thanks to the easier insertion in its tetragonal lattice [9,10]. In fact lithiation/delithiation mechanisms are different for the two polymorph. Both anatase and rutile polymorphs have a crystal structure consisting of TiO$_6$ octahedral and tetragonal symmetry, which forms channels for Li+ insertion. However, lithiation/delithiation reactions are easier in anatase structure. In rutile, belonging to *P42/mnm* space group, TiO$_6$ octahedra share edges in the c-direction and corners in ab-planes, while in anatase, with *I41/amd* space group, octahedra are distorted and share only four edges, forming a planar double chains. Therefore, while in rutile Li$^+$ diffusion occurs preferentially along c-axis channels, thus Li-Li repulsion inhibits rapidly Li insertion, in anatase Li$^+$ ions diffuse along the zig-zag channels connecting octahedral interstitial sites; in this case, Li-Li repulsive forces will result in the changing of symmetry to orthorhombic with only a small volume increasing [4,9,11].

Since rutile is the most stable polymorph, the anatase to rutile phase transition easy occurs at high temperature. It is a reconstructive transformation, since breaking and reconstruction of bonds take place, which lead to the contraction of c-axis in rutile lattice [12]. Such transformation is strongly dependent of a number of experimental parameters (i.e. temperature, reaction environment, particles size) therefore it is important to evaluate synthesis condition in order to favor the formation of only one polymorph [12,13].

In addition, the major drawbacks of TiO$_2$ are the small electronic and ionic conductivities: however, nano-sizing and nano-tuning morphologies are known ways to circumvent and overcome this issue [3,9,14].

Pulsed Laser Deposition (PLD) is a very promising technique to manufacture microelectrodes thanks to the ability to produce compact and dense films with a controlled thickness, the preservation of the ablation target stoichiometry in the final film composition and the capability to promote both amorphous or crystalline films by tuning the ablation/deposition parameters. Furthermore, PLD allows to deposit microelectrodes over a variety of substrates (metal, ceramics, wafer, polymers), in the form of single-component films, without any other typical electrode component such polymer binders, or as multi-layered composites by a fine tuning of the ablation/deposition conditions [15]. PLD has been successfully employed to manufacture both positive and negative thin film electrodes [1,16].

In this study PLD using a femtosecond-pulsed laser has been applied to anatase target materials to produce thin films of nanoparticles on aluminum substrates suitable for application as negative electrode in Li-ion MBs. The main drawback of PLD, in this case, was the obtaining of titania films composed of mixture of amorphous and crystalline phases, therefore different post-deposition treatments have been evaluated in order to drive a selective crystallization of anatase phase. Films morphology and composition have been investigated with a multi-technique approach and the corresponding performance and electrochemical properties in Li-ion MBs have been analyzed by cyclic voltammetry and galvanostatic techniques.

2. Materials and methods

PLD of anatase was carried out in a stainless steel vacuum chamber by the means of a frequency doubled (λ = 527 nm) Nd:glass laser (Twinkle-Light Conversion), with a pulse duration of 250 fs, repetition rate of 10 Hz and energy of 2.8 mJ. The target material was placed on a rotating holder, for avoiding the piercing, and the substrate was positioned in front of the target at a distance of 3 cm. The deposition was performed at ~10^{-4} Pa, room temperature (RT) for 3 h.The target material was obtained in form of pellet by cold pressing of anatase powder (99.8% of purity, from Aldrich) and following heat treatments in air at 500 °C for 2 h in a muffle, substrates were aluminum foil (Sigma-Aldrich) and monocrystalline silicon (Si (100)) wafer (GoodFellow). The films were subjected to different post deposition treatments as summarized in Table 1. Moreover, annealing treatment in air was carried out for 2 h not only at 500 °C, but also at 200 and 800 °C, in order to confirm that 500 °C is the proper temperature for TiO$_2$ films treatments.

Some deposited films were coated by a carbon layer applying a second PLD experiment. In this case a frequency doubled Nd:YAG was used as laser source (λ = 532 nm, τ = 7 ns, repetition rate = 10 Hz, fluence = 12 Jcm^{-2}), the target materials was graphite stick, the TiO$_2$ deposited-Al foil was used as substrate, kept at 3 cm for 10 min of deposition time.

In order to study the growth mechanism of fs-deposited films, transmission electron microscopy (TEM, Fei-TEC-NAI G2 20 TWIN) was performed. In this case, the substrate was aholey carbon-coated copper grids and the deposition time was 10 min.

Morphological characterization was made by the means of scanning electron microscope (SEM) (Philips, FEI ESEM XL30). Films crystallinity were verified by X-Ray diffraction (XRD) using a X-Perth-Pro (Philips) diffractometer in the following conditions: CuKα radiation (λ = 1.5405600 Å),2θ = 20° – 60°, step size 0.040°, time per step 4 s. Percentages of crystalline phases were estimated by performing by the Rietveld refinement using GSAS-II [17]. Spectroscopic characterization was carried out by FT-IR, Raman and XPS (X-Ray photoelectron spectroscopy) techniques. For FT-IR spectroscopy a Jasco FT-IR 460 Plus interferometer was used, collecting 100 scans at 4 cm^{-1} resolution, in the range of 4000–400 cm^{-1}. In this case, the substrate was a Si (100)) wafer. Micro-Raman measurements have been obtained using a DilorLabram micro-Raman spectrophotometer using a 632 nm excitation wavelength, a Peltier CCD camera detector and an 1800 gr mm^{-1} grating, a edge filter, which excludes Raman shift below 150 cm^{-1} from detection. All spectra have been acquired with an accumulation time of 60–120 s.

Electrochemical properties were studied by cycling voltammetry (CV) and galvanostatic techniques (GC). Electrochemical cells have been assembled in an ItecoEng SGS30 Ar-filled glove box with moisture content below 0.1 ppm. EL-CELL Std cells have been used as test cells for the electrochemical experiments. Thin film electrodes have been coupled with Whatman glass fiber separators and lithium disk counter electrodes (Sigma Aldrich). A 1 molal solution of LiPF$_6$ dissolved in a ethylene carbonate-dimethyl carbonate (EC:DMC) solvent blend (1:1 in volume) has been used as electrolyte (Solvionic). The TiO$_2$ mass loading on the aluminum electrode support is approximately 0.2 mg cm^{-2}. Currents and capacities have been set in respect to the geometric size of the microelectrodes: the corresponding approximate gravimetric values have been calculated by using the mean electrode mass loading obtained in PLD estimated on 10 different electrodes. CV tests have been carried out using the Ivium Vertex potentiostat/galvanostat/FRA device whereas GC experiments have been carried out using an 8-channel MTI battery test system. Ex situ Raman spectroscopy analysis have been carried out on samples collected *post mortem* from lithium half cells. Cells have been de-assembled in the Ar-filled glove box and electrodes recuperated. Materials have been washed carefully in DMC (twice), tetrahydrofuran and
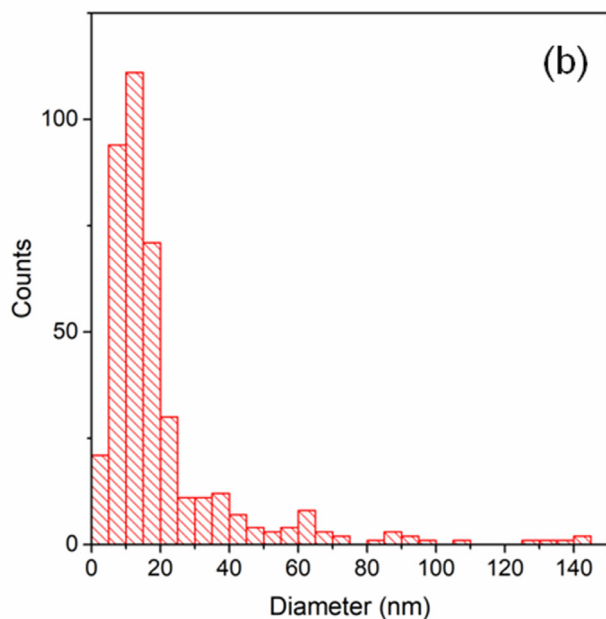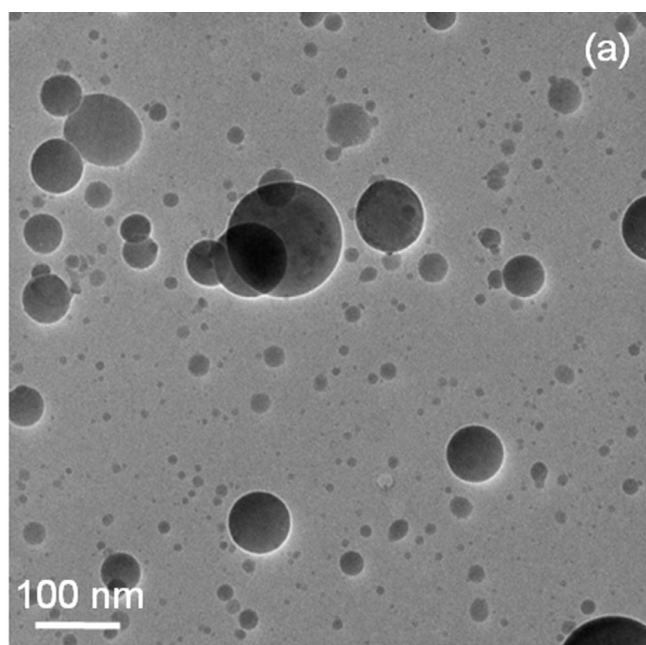
Fig. 1. TEM image registered on TiO$_2$ deposited for 12 min (a) and particles size distribution obtained from different TEM images (b).

then dried out overnight in dynamical vacuum at room temperature. Electrodes have been inserted in an in-house-made sealed holder with a glass optical window to preserve the materials from air contamination during the Raman analysis.

3. Results and discussion

3.1. Thin films characterization

A TEM micrographyrecorded on a PLD deposition on aholey carbon-coated copper grid is shown in Fig. 1(a) to study the elementary nanoparticles (NPs) that constitute the thin film electrode: the size distribution analysis obtained on several TEM micrographs is presented in the Fig. 1(b). Films are constituted by round-shaped NPs characterized by a mean diameter of about 20 nm, while only some larger particles
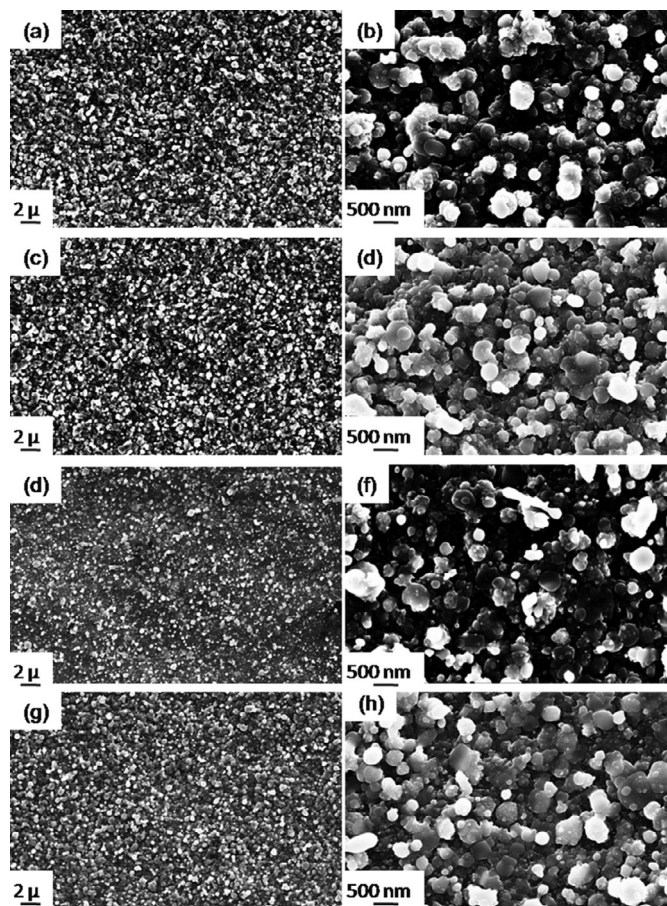
Fig. 2. SEM images acquired at two different magnification on TO01 (a, b), TO02 (c, d), TO03 (e, f) and TO04 (g,h) films.

of ~100 nm are observable (Fig. 1(b)). This is an expected morphology for thin films obtained by fs-PLD in vacuum [18]. In fact, it has been already demonstrated that the emission of NPs typically occurs during a PLD experiment conducted in ultra-short regime and represent the main components of the deposited films [18–22].

SEM images registered on the thin films at two different magnification are reported in Fig. 2. Irrespective of the post-deposition treatment, all the films are uniform and formed by the coalescence of a large number of NPs, as already observed for other films deposited by ultra-short PLD technique [20–22]. SEM images demonstrate a dense, compact, crack-free and nanostructured morphology without relevant inhomogeneities in the micro-range. All these morphological features are necessary pre-requisites for thin film electrode materials. Homogeneity and compactness should provide a uniform electrochemical behavior over the film surface, whereas the nanosized particles may provide improved TiO$_2$ performance with respect to the bulk form.

The thin film crystallinity has been checked by XRD. The patterns of TO01, TO02, TO03 and TO04 are shown in Fig. 3(a) in comparison with the target one. To estimate the percentages of anatase and rutile phases Rietveld analyses were carried out. The as deposited film without thermal post-treatments (i.e. TO01) is characterized by the presence of both anatase (59±10%) and rutile (41±10%) phases (PDF 01–071–1167 and PDF 00–034–0180, respectively), while the target materials is mainly found in anatase phase, presenting only a negligible contribution of rutile. The phase transformation of anatase to rutile is not surprising during the fs-PLD because ablated materials can reach remarkably high temperatures inside the plasma phase (thousands of Kelvins) [20–22], where rutile phase can be obtained. Annealing treatments were carried out in order to improve film crystallinity. After annealing in air at 500 °C
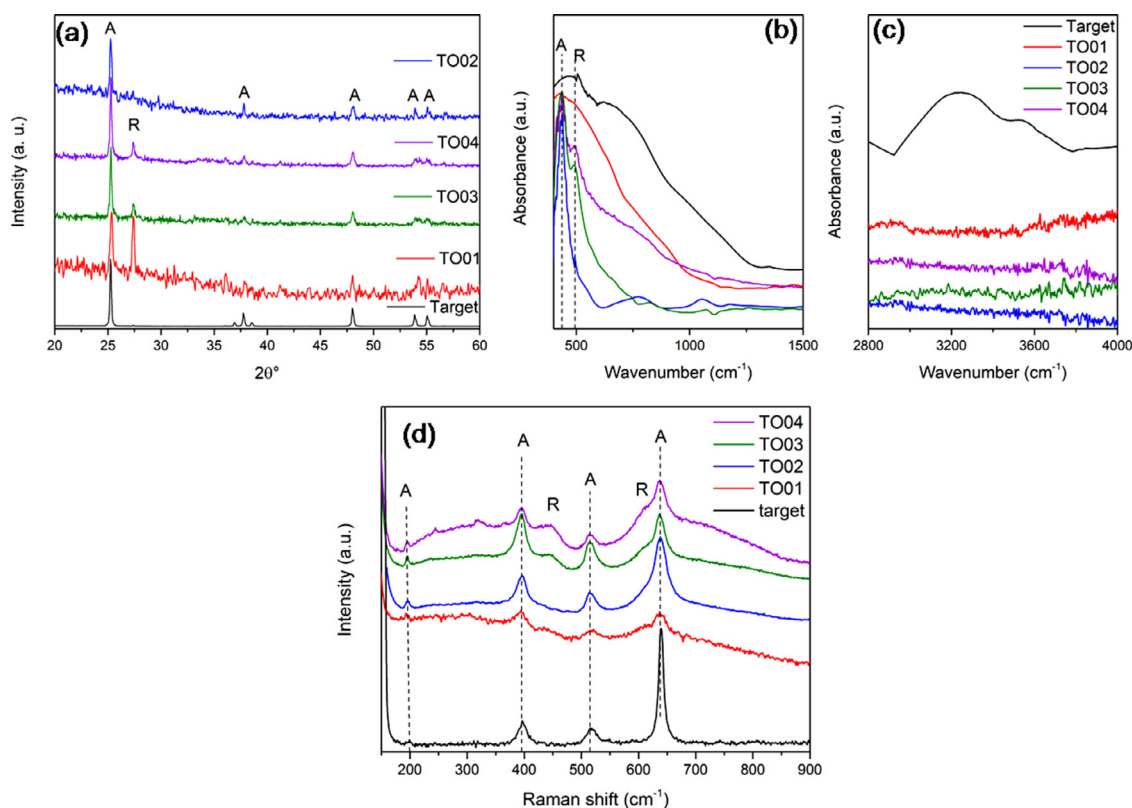
Fig. 3. Normalized XRD patters (a), FTIR (b, c) and Raman (d) spectra of the thin film electrodes compared to the target material, where "A" and "R" denote anatase and rutile, respectively.

only anatase (92±11%) peaks are clearly detectable, while after annealing in Ar flux a small percentage of rutile (31±8% and 29±8% for TO03 and TO04, respectively) is still present. The crystallite sizes estimated using Scherrer equation [23] show only a slight increase of the particle dimension after heat treatments. Scherrer formula was applied on the peak at $2\theta°$ 25.27, corresponding to (101) planes of anatase, and at $2\theta°$ 27.44, corresponding to (110) planes of rutile. In TO01 calculated crystallite size are 28 and 31 nm for anatase and rutile, respectively, while in TO02, TO03 and TO04 the anatase one is of 35, 48 and 46 nm, respectively.

FTIR spectra shown in Fig. 3(b) exhibit distinctive signals of TiO_2 [24,25]. The target spectra shows a broad band between 400 and 800 cm^{-1}, where it is possible to identify the stretching of Ti–O and Ti–O–Ti (bridging stretching) around 470 and 700 cm^{-1}. TO01 spectrum shows a broad band in the same wavenumber range, while a characteristic peak of anatase polymorph is observable at 434 cm^{-1} [13] in TO02 spectrum. TO03 and TO04 show both anatase and rutile main peaks at 434 and 493 cm^{-1} [13]. Hydroxyl stretching vibration bands can be identified only in the target spectra, in the range 3000–3700 cm^{-1} (Fig. 3(c)), whereas surface OH groups or adsorbed H_2O are apparently absent on thin film electrodes [26,27].

In Fig. 3(d) Raman spectra of target material and TiO_2 films are shown, while peaks assignments are reported in Table 2. Here only the tail of the main Raman signal, related to the strongest E_g mode of anatase, is visible since it is very close to the edge filter cut-off at 150 cm^{-1}. Very weak signals are visible in TO01 due to the more amorphous character of the film before the heat treatments, after which their intensities increase, indicating the enhancement of crystallinity. In films spectra both anatase and rutile peaks are visible, in all the cases rutile modes originate only weak and broad bands at 445 and 604 cm^{-1}, overlapped by anatase peaks centered at 396 and 639 cm^{-1}, respectively. It is important to underline that anatase peaks in these positions have a much smaller Raman cross section than rutile [28], therefore one may

Table 2
Observed Raman signals and their assignment.

Phase	Raman shift (cm^{-1})	Assignment [28,29]
Anatase	195	E_g
	396	B_{1g}
	515	$A_{1g}+B_{1g}$
	639	E_g
Rutile	445	A_{1g}
	604	B_{2g}

speculate that rutile content is very smaller than anatase, especially in TO02 sample where rutile is detectable only as a small shoulder of the anatase peak at 639 cm^{-1}.

All the characterization techniques demonstrate the effective recrystallization of the deposited films during heat treatments at 500 °C. Besides it has been demonstrated that rutile starts to crystallize at temperature around 600 °C, numerous studies have been devoted to understand the crystallization behavior of titania polymorphs in relation to the particles size [12,13,30–32]. On the bases of these studies, after the estimate of nanometer-scale particles dimensions from TEM images, a temperature of 500 °C was chosen to drive the crystallization of the deposited materials in an anatase phase during post-deposition heat treatments. Moreover, to support this choice, annealing in air was carried out at different temperatures 200, 500 and 800 °C in order to find the temperature at which anatase phase crystallizes predominantly. The normalized diffraction patterns, reported in Fig. S1, show how the relative intensities of the main peak of anatase and rutile change with the annealing temperature. No substantial differences can be observed between the as deposited film and the sample treated at 200 °C; the annealing at 500 °C lead to the crystallization of only anatase phase while at 800 °C both anatase and rutile phases crystallize. All these results confirms the study on anatase to rutile phase transition carried out
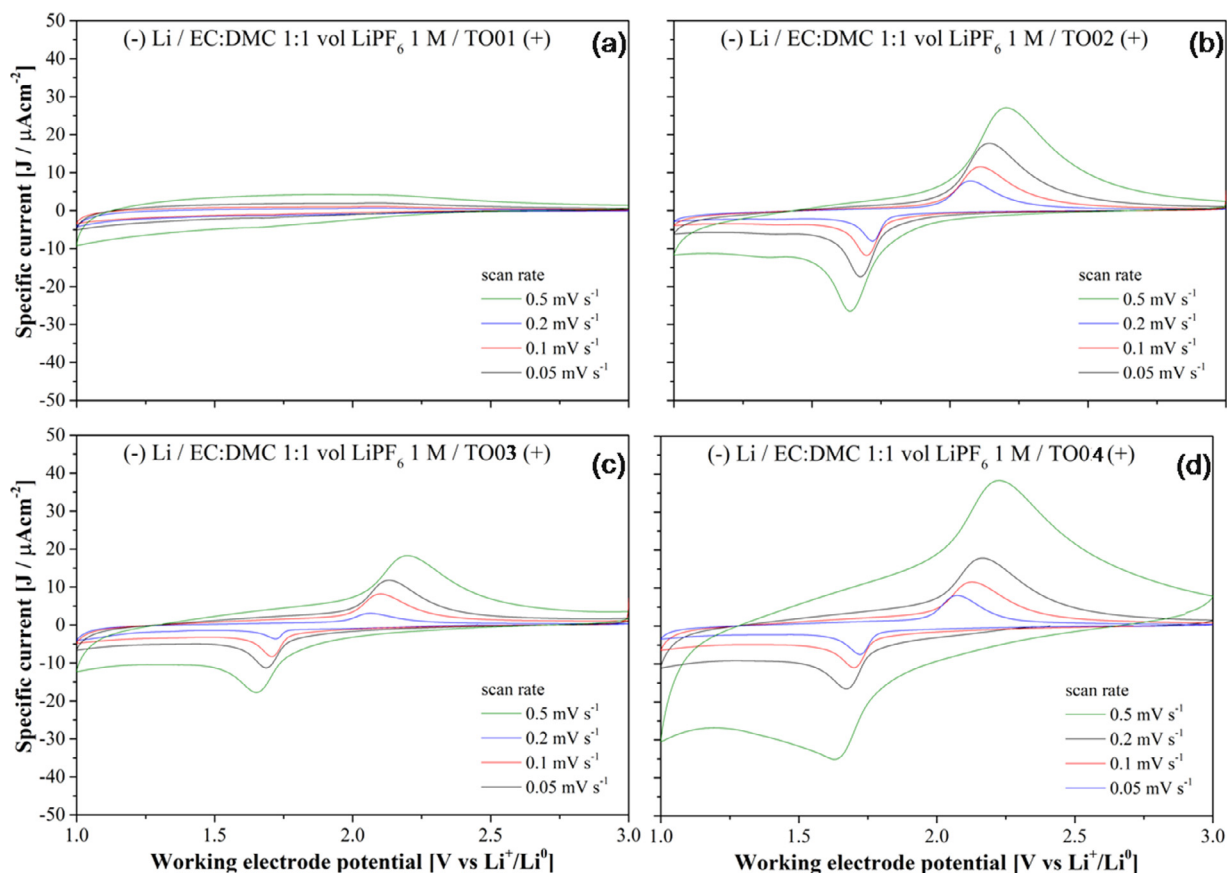
Fig. 4. CV profiles registered at different scan rate for TO01 (a), TO02 (b), TO03 (c) and TO04 (d).

by Djaoued and coworkers [13] in nanocrystalline TiO$_2$ polymorphs, which demonstrated that films treated at temperature < 500 °C were amorphous, while anatase crystallization occurs at 500 °C and at 800 °C a mixture of anatase and rutile were observed.

Although rutile is the most stable titania polymorph, the choose to promote anatase crystallization is due to the poorer rutile's electrochemical activity in Li-ion batteries both in bulk and nanoparticles forms [11]: diffusion path and lithiation/delithiation mechanism are different for the two polymorph.

Once experimental conditions for promoting crystallization of TiO$_2$ in anatase phase were found, a carbon coating for the further improving of electrochemical has been also realized (TO04).

3.2. Electrochemical characterization

The electrochemical activity of thin film electrodes have been tested in lithium half cells. CV tests registered at different scan rates are shown in the Fig. 4 for the TO01, TO02, TO03 and TO04 thin film electrodes.

With exception of TO01, which shows poor electrochemical activity, all the thin film electrodes shows the expected CV fingerprint of the reversible lithium intercalation in the anatase tetragonal lattice with a single anodic/cathodic peak centered at about 1.8 V *vs.* Li. It is remarkable that the CV shape is preserved even at high scan rates for all the annealed material, thus suggesting that Li-ion insertion/extraction to/from TiO$_2$ thin films is kinetically highly reversible. Overall, heat treatments enhance the electrochemical activity. The comparison between TO02 and TO03 suggests that post-deposition air heat treatments are more effective (TO02 in Fig. 4(b)) compared to Ar-annealing (TO03 in Fig. 4(c)). On the other hand, the deposition of a carbon layer (TO04) followed by Ar-annealing boosts the electrochemical activity in CV outperforming all the other thin film electrodes.
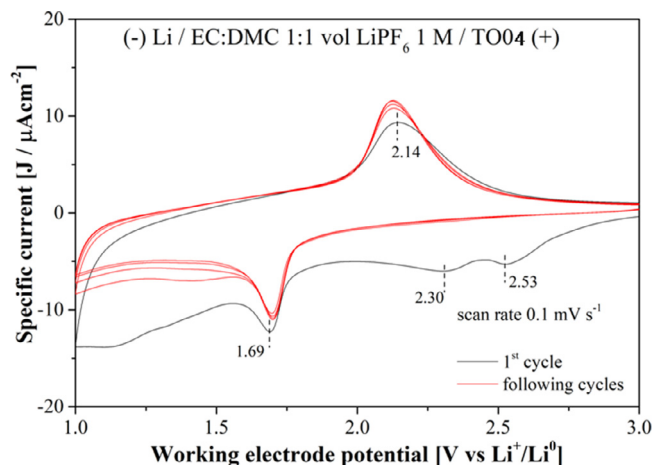

Fig. 5. CV test performed on the TO04 sample.

It is to be noted that the CV test performed on the TO04 sample shows in the first electrochemical lithium insertion/de-insertion two additional reductive peaks (cathode branch, see Fig. 5). These two additional electroactive processes are absent in all the other materials and are likely due to irreversible reduction reactions of the C-coating deposited on the surface of the TiO$_2$ film. In fact these processes are observed only in the first reduction of the CV scan of the TO04 samples whereas are absent in all the subsequent cycles.

By applying the Randless-Sevcik equation [33] to the CV data shown in the Fig. 4, it is possible to estimate the diffusion coefficient of lithium ions (D$_{Li}$) in the anatase (cathodic peaks) and titanate (anodic
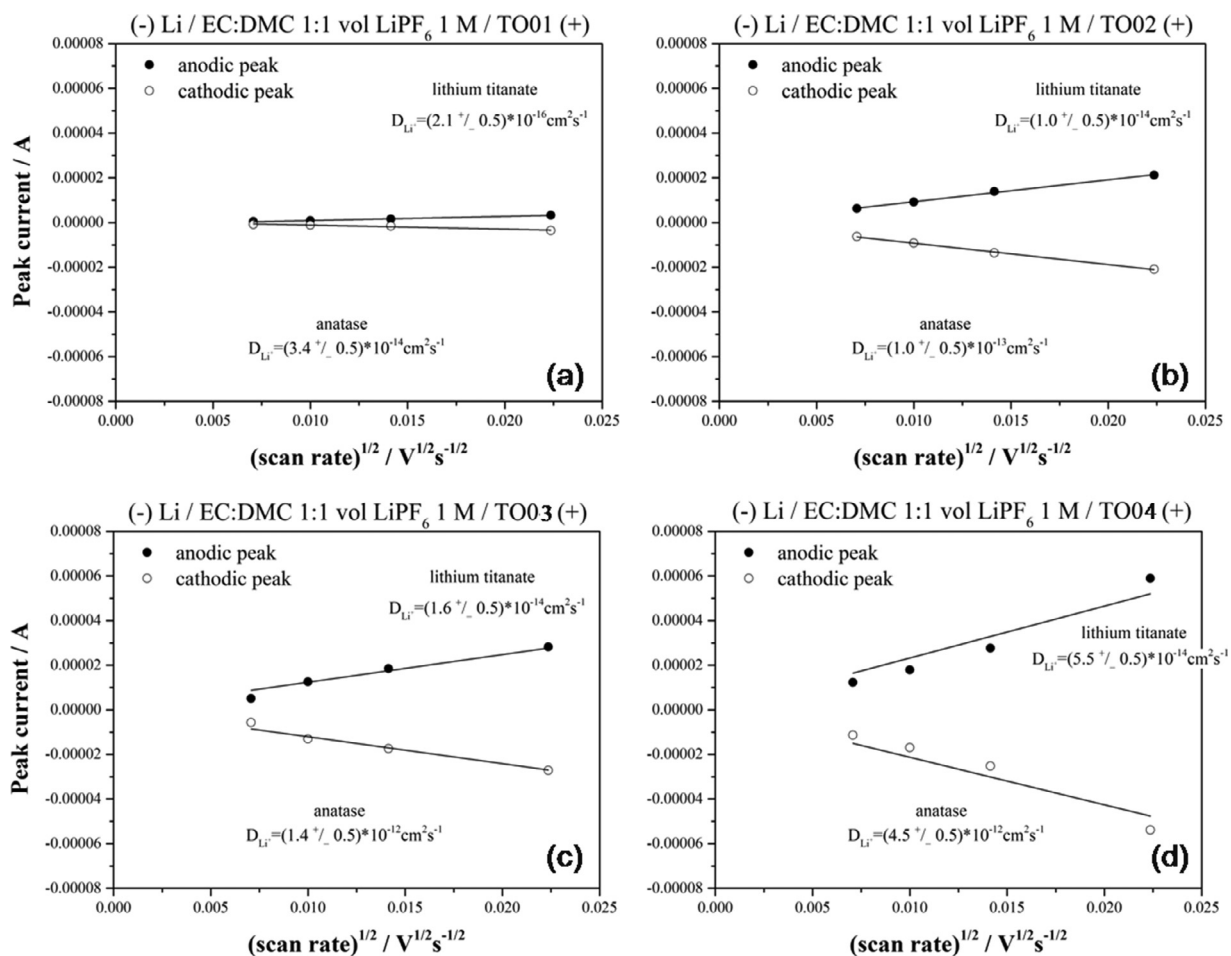
Fig. 6. Anodic and cathodic current peak *vs.* square root of scan rates for TO01 (a), TO02 (b), TO03 (c) and TO04 (d).

peaks) lattices. We estimated a Li$^+$ concentration being 2.4×10^{-3} and 2.4×10^{-2} mol cm^{-3} for the anatase and titanate lattices, respectively. These values have been calculated by assuming a 5% lithium ion solubility in the pristine Li$_x$TiO$_2$ tetragonal lattice of anatase and a Li$_{\frac{1}{2}}$TiO$_2$ stoichiometry for the orthorhombic titanate lattice, in line with the available literature concerning the lithium intercalation mechanism [8,34].

The linear plot of peak current values *vs.* scan rate for the four thin film electrodes are shown in the Fig. 6.

The apparent D$_{Li}$ values in lithium titanate were 2.1×10^{-16}, 1.0×10^{-14}, 1.6×10^{-14} and 5.5×10^{-14}cm^{2}s^{-1} whereas in anatase were 3.4×10^{-14}, 1.0×10^{-13}, 1.4×10^{-12} and 4.5×10^{-12}cm^{2}s^{-1}, for TO01, TO02, TO03 and TO04, respectively. Larger D$_{Li}$ values have been obtained in nano-anatase compared to the titanate phases due to the larger number of empty octahedral-intercalation sites in the anatase lattice compared to the Li$_{\frac{1}{2}}$TiO$_2$ titanate where half atomic sites are occupied by definition by Li$^+$ ions: this evidence is in line with the literature [7].

The lithium diffusion coefficient of nano-anatase is in thin film materials larger compared to the expected value for bulk anatase, whose value is of about 10^{-16} cm^{2}s^{-1} [3], thus confirming the beneficial impact of nanosizing of the electrochemical transport properties of TiO$_2$. Moreover, post-deposition heat treatments further enhance the lithium diffusion coefficient in nano-anatase by at least one order of magnitude compared to as deposited films (TO01). A similar trend is also observed for the lithium diffusion coefficient in the Li$_{\frac{1}{2}}$TIO$_2$ titanate (discharged electrodes) where increases of more than 2 orders of mag-

nitudes is achieved for all film submitted to post-deposition annealing. This enhancement can be related to the crystalline structural changes from a mixture of rutile and anatase phase embedded in an amorphous matrix in TO01 to a predominant and well crystallized anatase phase after heat treatments, confirming the easier Li$^+$ diffusion path in anatase polymorph [4,9,11]. On passing it is interesting to recall that Wagemaker et al. [35] studied Li$^+$ diffusion in microcrystalline anatase by ^{7}Li magic angle spinning solid-state NMR, obtaining a value for the diffusion coefficient of 4.7×10^{-12} cm^2 s^{-1} a value 4 orders of magnitude larger compared to the assessed value for anatase [3]. Wagemaker suggests that larger values in the lithium diffusion coefficient in anatase are usually obtained with NMR with respect to electrochemical methods since they are not affected by surface effects as well as grain and crystallographic phase boundaries. In this view one may speculate that in PLD thin films annealed at 500 °C the transport hindrance of Li$^+$ opposed by grain boundaries is mitigated.

The lithium diffusion coefficients for all annealed materials are close, or in some cases larger, to those reported in literature for other TiO$_2$ thin films. Fu and Qin [36] reported two different values of D$_{Li}$ of 1.4×10^{-13} and 6×10^{-14} cm^2 s^{-1} for a ns-pulsed laser deposited anatase film estimated by cyclic voltammetry and potential step, respectively. Lindström et al. [37] estimated D$_{Li}$ of 2×10^{-15} cm^{2}s^{-1} in an anatase films produced by CVD using chronoamperometry. Lakshmi-Narayana et al. [7] measured from cyclic voltammetry measurements a D$_{Li}$ of 1.1×10^{-14} cm^{2}s^{-1} on an anatase film obtained by electron beam deposition.

Our promising values for the lithium ion transport properties are a clear indication that fs-PLD followed by heat treatments is a suitable method for the production of nanostructured anatase films for MB appli-
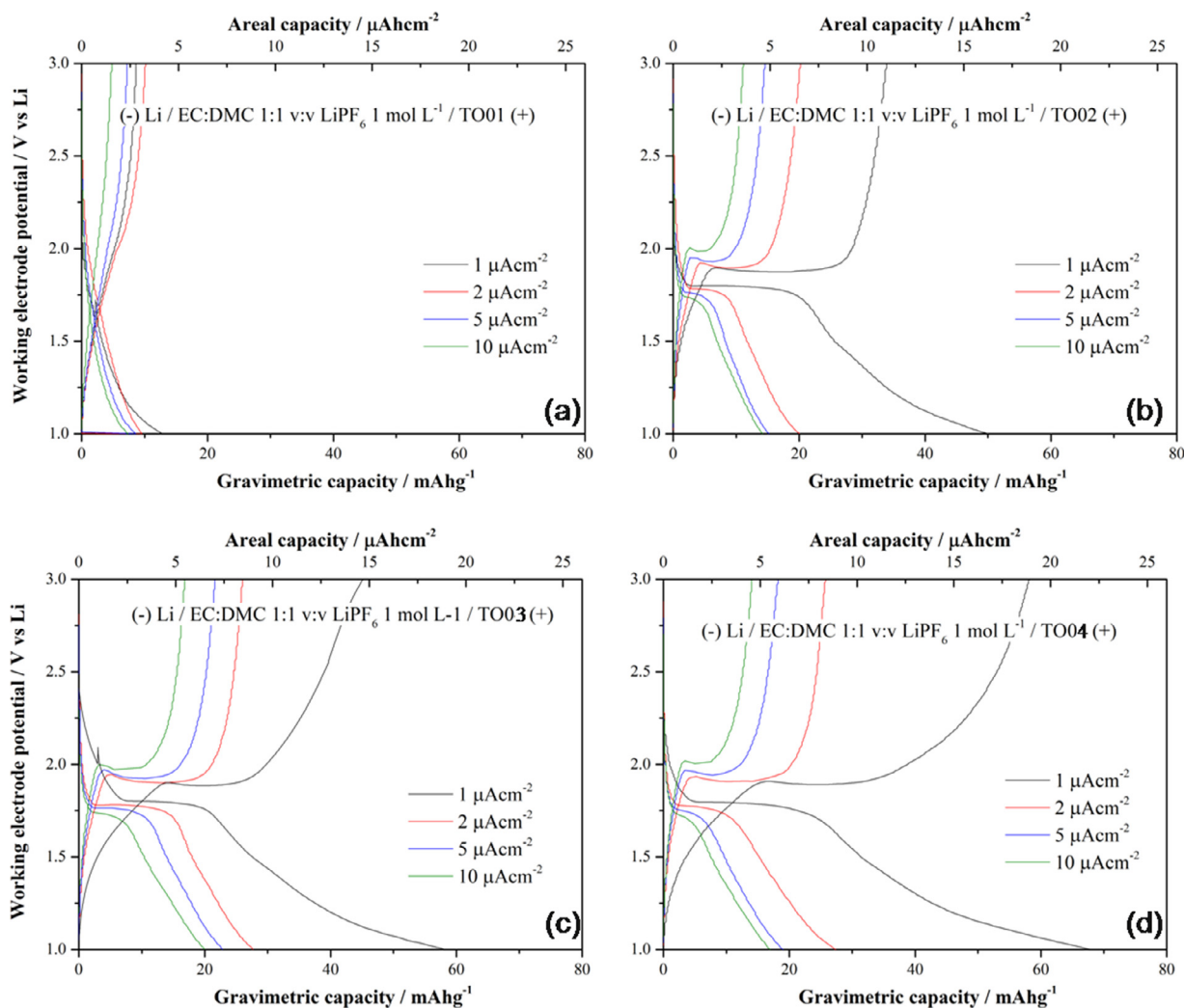
Fig. 7. Voltage profile of lithium cell assembled using the TO01 (a), TO02 (b), TO03 (c) and TO04 (d) laser deposited electrodes.

cation. Furthermore, in presence of a carbon layer (TO04), D_{Li} increases by 3–4 times in the anatase lattice and by 4–5 times in the lithium titanate lattice compared to the other annealed materials in line to previous observation reported in the literature about the beneficial impact of a carbonaceous film on Li transport properties [4].

The performance of lithium half cells of all the thin film electrodes has been measured in galvanostatic cycling at various current rates as shown in the Fig. 7.

Again in the CG tests the TO01 thin films show poor electrochemical activity suffering very large overpotentials. On the other hand, in line with previous data by CV, Ar and Air heat treatments at 500 °C boost the performance (TO02, TO03 and TO04). In addition, at 1 μAcm^{-2} the carbon coated anatase thin film (TO04) is able to reversibly cycle approximately 41% of the theoretical capacity of the electrode, confirming as the carbon layer improves the electrochemical performances of the anatase electrode. Overall the TO04 sample overcomes all the other thin film electrodes in terms of performance in line with the improved transport properties derived by CV (see above).

All the voltage profiles, except for TO01 (Fig. 7(a)), show the typical fingerprint of anatase electrodes: after the initial limited lithiation with a solid-solution mechanism, corresponding to the first voltage slope in lithiation/delithiation curve from open circuit potential (OCP) to approximately 1.8 V *vs.* Li, the anatase lattice undergoes to the orthorhombic distortion causing the deformation of the octahedral coordination of Ti resulting in a phase separation into $Li_{0.05}TiO_2$ (tetragonal) and

$Li_{0.5}TiO_2$ (orthorhombic), visible as voltage plateau, finally a second solid-solution step occurs (second voltage slope) [8,11]. In particular, in discharge TO02, TO03 and TO04 show a plateau in the galvanostatic potential profiles at about 1.8 V *vs.* Li followed by a smooth slope at smaller potential, while upon charge a stable plateau is at about 1.9 V (longer compared to the corresponding plateau in discharge) followed by a steep slope. On the contrary in the TO01 thin film the electrochemical behavior is less clear and the voltage profiles is similar to rutile, where a continuous voltage slope is observable as a result of a solid solution formation during the lithiation/de-lithiation in rutile lattice [8].

The Tafel plots derived from the galvanostatic data are shown in the Fig. 8.

The intersection between the two linear trends outlined in all Tafel plots gives estimates of the thermodynamic reduction potential E° and the electrochemical exchange current J°, that further allow to calculate the charge transfer resistance of the electrochemical process in the small polarization approximation ($R_{ct} = RT/J°F$, where R is the Gas constat, T is the absolute temperature, and F is the Faraday constant).

The estimated Ti^{4+}/Ti^{3+} E° is 1.55 V *vs.* Li in TO01 whereas in all the other material is 1.83 V *vs.* Li. The electrochemical redox potential for the reduction of titanium oxide, E°, falls in the range 1.5–1.8 *vs.* Li depending on the TiO_2 polymorph: the expected value for the lithiation of anatase is ~1.8 V *vs.* Li is in line with our observations [3]. Again, the different behavior of TO01 with respect to the other materials is attributable to the more amorphous character of the film together with
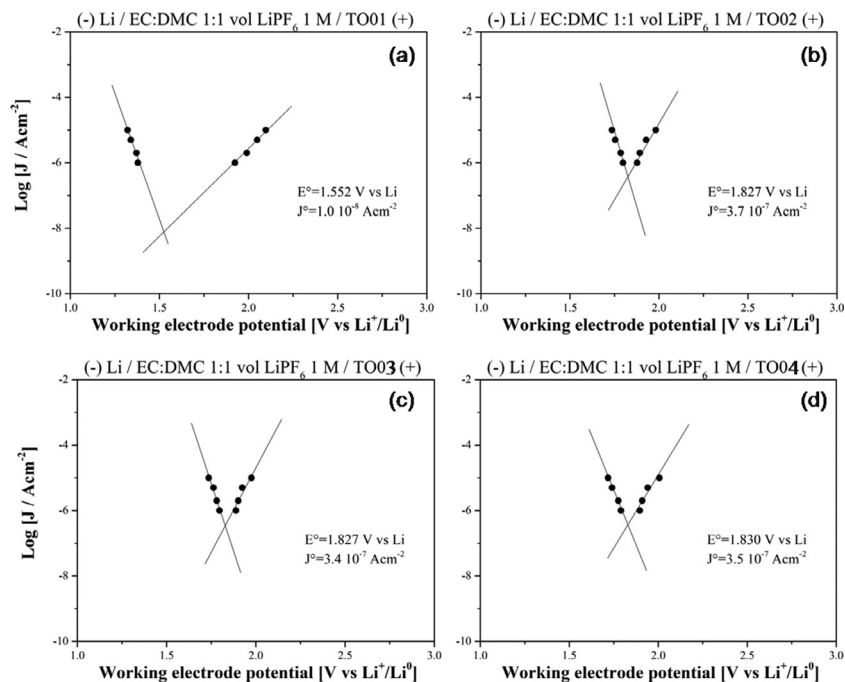
Fig. 8. Tafel plots obtained by galvanostatic cycling of lithium cell assembled using the TO01 (a), TO02 (b), TO03 (c) and TO04 (d) laser deposited electrodes.
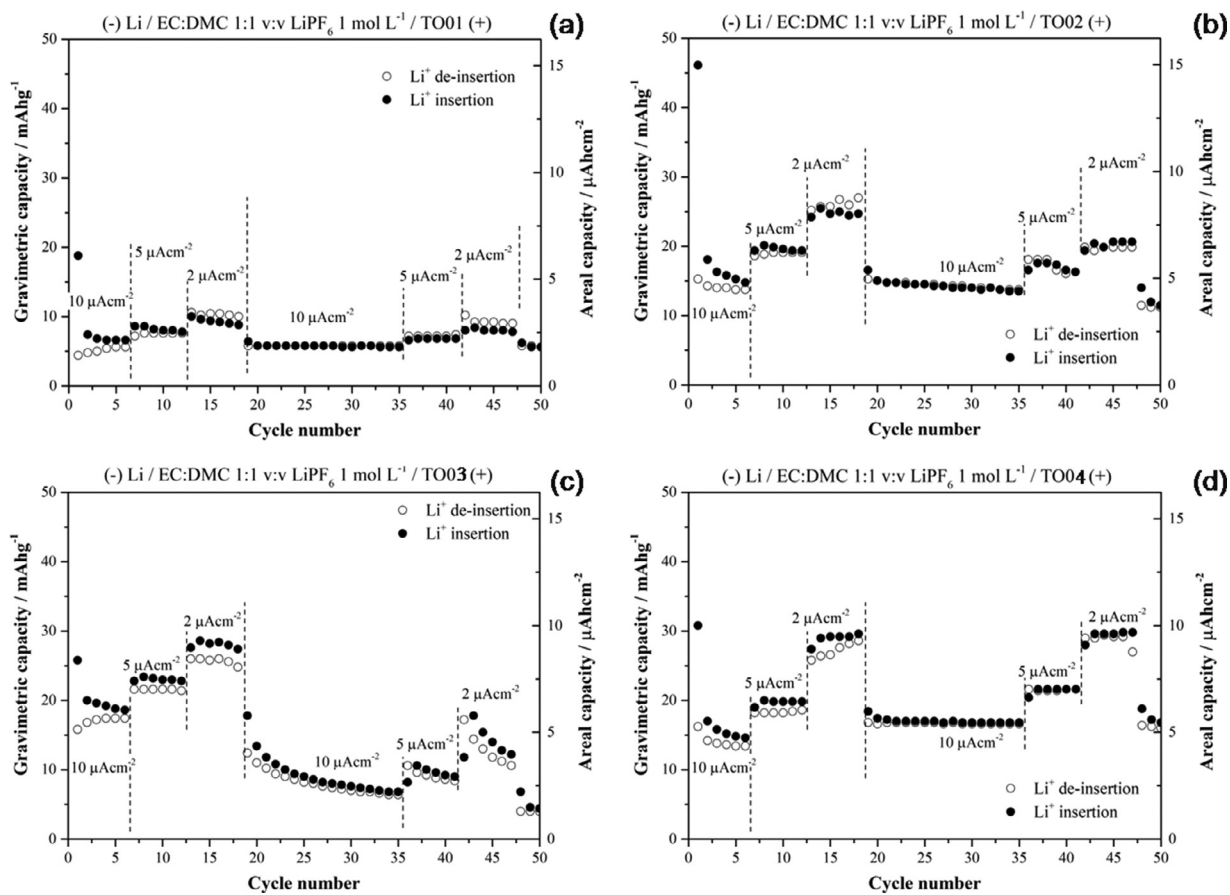

Fig. 9. Cycle performance at various current rate of the TO01 (a), TO02 (b), TO03 (c) and TO04 (d) laser deposited electrodes.
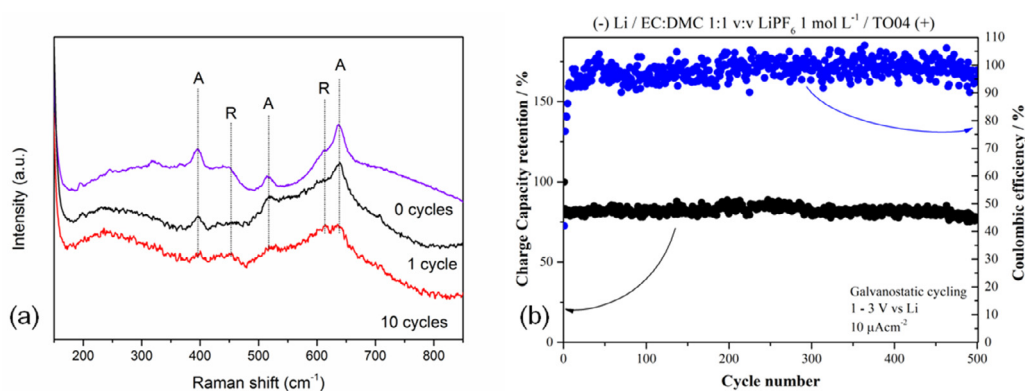
Fig. 10. Raman spectra acquired on TO04 as deposited and after 1 and 10 cycles, where "A" and "R" denote anatase and rutile, respectively (a), evolution of charge capacity retention and coulombic efficiency upon cycling (b).

the presence of mixed rutile and anatase phases and possibly to the poor transport properties that induces remarkable overpotentials.

Turning to the charge transfer resistance, TO02, TO03 and TO04 materials show a increase of more than 1 order of magnitude of J° compared to TO01, and thus a decrease in the R_{ct} value by 1 order of magnitude is predictable for all the annealed materials.

The cycle performance of all the thin film electrodes in CG tests is shown in the Fig. 9.

All samples show a reversible electrochemical performance upon cycling in galvanostatic conditions: as expected all annealed thin film electrodes outperform the pristine TO01 one. The comparison between TO02 and TO03 suggest that the Air annealing leads to a better reversibility compared to the Ar annealing treatment. On the other hand, the C-coated material (TO04) annealed under Ar outperforms all the other electrodes in terms of reversibility and capacity retention upon cycling.

However, apart the excellent reversibility and cycling stability, TO02 suffers of a poor coulombic efficiency (CE) in the first galvanostatic cycle compared to all other materials, being the CE the ratio between discharge and charge capacities at a given cycle number. This is not unexpected and is originated by the spontaneous degradation of the electrolyte over the pristine surface of TiO_2 [38]. Apparently, the annealing under Ar mitigates this detrimental effect, possibly thanks to the removal of the residual protons absorbed (e.g. TO03 and TO04). On the other hand, the Ar annealing it is expected to lead to oxygen losses at 500 °C thus forming Ti^{3+} centers on the surface [32]: further experimental activity is in progress to confirm this point. Overall, the Ar annealing itself mitigates the irreversible capacity in the first cycle but leads to a material with worse reversibility. The TO04 material is in this respect a compromise where the carbon coating acts not only as a conductive media that improves the charge transfer and ion diffusion, but also as a protective layer that preserves the integrity of the TiO_2 anatase material upon annealing and cycling [4]. An experimental validation of this hypothesis is presented in the Fig. 10(a), where the Raman spectra of TO04 electrodes recuperated after cycling in lithium half cells are compared.

In agreement with our previous speculations, the Raman spectra confirm the vibrational fingerprint of the anatase lattice after 1 and 10 cycles in battery.

As a final point, also the long-term cycling stability of TO04 has been demonstrated by recording a GC test for 500 cycles at 10 μAcm^{-2}, the remarkable performance is shown in Fig. 10(b). The charge capacity retention is higher than 75% after 500 cycles, whereas the mean coulombic efficiencies are above 98% after approximately 50 cycles.

4. Conclusions

Compact and dense TiO_2 films composed by nanoparticles were obtained by ultra-short pulse laser deposition of an anatase target. The films are characterized by the presence of both anatase and rutile phases embedded in an amorphous matrix. Since the anatase polymorph shows superior electrochemical properties, thermal post-deposition treatments were evaluated. The annealing at temperature of 500 °C promote the crystallization of the anatase polymorph. As a result heat-treated films shows distinctive characteristics of anatase phase both in physicochemical characterization and electrochemical tests. Despite the deposition of TiO_2 films by fs-PLD leads to thin film electrodes that are electrochemically almost inactive in lithium half cells, post deposition annealing (either in Ar or Air) boosts the electrochemical activity; in particular air annealing outperforms Ar annealing. Annealed materials show an increase in both the diffusion coefficient and a decrease in the charge transfer resistance. A further improvement in the electrochemical performance and properties is obtained by the deposition of a carbon layer over the TiO_2 thin film followed by annealing under Ar. This TiO_2/C layered microelectrode morphology leads to multiple beneficial effects compared to the benchmark microelectrodes:

- It increases the apparent Li^+ diffusion coefficient both in the anatase and the lithium titanates.
- It decreases the charge transfer resistance of the Ti^{4+}/Ti^{3+} redox couple.
- It improves the capacity retention upon cycling.

In summary the ability of fs-PLD to produce single layer or multi-layer titanium oxide thin film electrodes for Li-ion MB has been demonstrated. Moreover, the favorable effect of a carbon coating obtained with only ten min of laser deposition has been proved. Further studies are in progress to evaluate the impact of the nature of the carbon coating on the electrochemical properties of TiO_2 microelectrodes. Moreover, additional characterization techniques of reversibility should be evaluated (i.e. in situ Raman spectroscopy [38] and in situ XRD [39,40]).

Declaration of Competing Interest

The authors declare that they have no known competing financial interests or personal relationships that could have appeared to influence the work reported in this paper.

Supplementary materials

Supplementary material associated with this article can be found, in the online version, at doi:10.1016/j.apsadv.2021.100090.

References

[1] C.M. Julien, A. Mauger, Pulsed laser deposited films for microbatteries, Coatings 9 (2019) 386, doi:10.3390/coatings9060386.

[2] J.H. Pikul, P.V. Braun, W.P. King, Performance modeling and design of ultra-high power microbatteries, J. Electrochem. Soc. 164 (2017) 11 E3122-E3131, doi:10.1149/2.0151711jes.

[3] M. Fehse, E. Ventosa, Is TiO2(B) the future of titanium-based battery materials? Chempluschem 80 (2015) 785–795, doi:10.1002/cplu.201500038.

[4] M. Madian, A. Eychmüller, L. Giebeler, Current advances in TiO_2-based nanostructure electrodes for high performance lithium ion batteries, Batteries 4 (2018) 7, doi:10.3390/batteries4010007.

[5] D.M. Cunha, T.A. Hendriks, A. Vasileiadis, C.M. Vos, T. Verhallen, D.P. Singh, M. Wagemaker, M. Huijben, Doubling reversible capacities in epitaxial $Li_4Ti_5O_{12}$ thin film anodes for microbatteries, ACS Appl. Energy Mater. 2 (2019) 3410–3418, doi:10.1021/acsaem.9b00217.

[6] A. Mauger, H. Xie, C.M. Julien, Composite anodes for lithium-ion batteries: status and trends, Mater. Sci. 3 (3) (2016) 1054–1106, doi:10.3934/matersci.2016.3.1054.

[7] A. Lakshmi-Narayana, L. Zhang, C. Jiao, C.M. Julien, Y. Qiu, TiO_2 thin films on Au/Ti/SiO2/textured Si substrates as high capacity anode for Li-ion batteries, Ceram. Int. 46 (2020) 10299–10308, doi:10.1016/j.ceramint.2020.01.024.

[8] M. Søndegaard, Y. Shen, A. Mamakhel, M. Marinaro, M. Wohlfrahrt-Mehrens, K. Wonsyld, S. Dahl, B.B. Iversen, TiO_2 nanoparticles for Li-ion battery anodes: mitigation of growth and irreversible capacity using LiOH and NaOH, Chem. Mater. 27 (2015) 119–126, doi:10.1021/cm503479h.

[9] Z. Yang, D. Choi, S. Kerisit, K.M. Rosso, D. Wang, J. Zhang, J.Liu G.Graff, Nanostructures and lithium electrochemical reactivity of lithium titanites and titanium oxides: a review, J. Power Sources 192 (2) (2009) 588–598, doi:10.1016/j.jpowsour.2009.02.038.

[10] D. Su, S. Dou, G. Wang, Anatase TiO_2: better anode material than amorphous and rutile phases of TiO_2 for Na-ion batteries, Chem. Mater. 27 (2015) 6022–6029, doi:10.1021/acs.chemmater.5b02348.

[11] V. Aravindan, Y.-.S. Lee, R. Yazami, S. Madhavi, TiO_2 polymorphs in 'rocking-chair' Li-ion batteries, Mater. Today 18 (6) (2015) 345–351, doi:10.1016/j.mattod.2015.02.015.

[12] D.A.H. Hanaor, C.C. Sorrell, Review of the anatase to rutile phase transformation, J. Mater. Sci. 46 (2011) 855–874, doi:10.1007/s10853-010-5113-0.

[13] Y. Djaoued, S. Badilescu, P.V. Ashrit, D. Bersani, P.P. Lottici, J. Robichaud, Study of anatase to rutile phase transition in nanocrystalline titania films, J. Sol Gel Sci. Technol. 24 (2002) 255–264, doi:10.1023/A:1015357313003.

[14] S. Moitzheim, B. Put, P.M. Vereecken, Advances in 3D thin-film li-ion batteries, Adv. Mater. Interfaces 6 (2019) 1900805, doi:10.1002/admi.201900805.

[15] D. Fujimoto, N. Kuwata, Y. Matsuda, J. Kawamura, F. Kang, Fabrication of solid-state thin-film batteries using $LiMnPO_4$ thin films deposited by pulsed laser deposition, Thin Solid Films 579 (2015) 81–88, doi:10.1016/j.tsf.2015.02.041.

[16] A. Smaldone, S. Brutti, A. De Bonis, N. Ciarfaglia, A. Santagata, R. Teghil, Iron doped LiCoPO4 thin films for lithium-ion microbatteries obtained by ns pulsed laser deposition, Appl. Surf. Sci. 445 (2018) 56–64, doi:10.1016/j.apsusc.2018.03.168.

[17] B.H. Toby, R.B. Von Dreele, GSAS-II: the genesis of a modern open-source all purpose crystallography software package, J. Appl. Cryst. 46 (2013) 544–549, doi:10.1107/S0021889813003531.

[18] S. Amoruso, G. Ausanio, R. Bruzzese, M. Vitiello, X. Wang, Femtosecond laser pulse irradiation of solidtargets as a general route to nanoparticle formation in a vacuum, Phys. Rev. B 71 (2005) 033406, doi:10.1103/PhysRevB.71.033406.

[19] J. Perriere, C. Boulmer-Leborgne, R. Benzerga, S. Tricot, Nanoparticle formation by femtosecond laser ablation, J. Phys. D 40 (2007) 7069–7076, doi:10.1088/0022-3727/40/22/031.

[20] A. De Bonis, R. Teghil, J.V. Rau, A. Galasso, S. Orlando, A. Santagata, Characterization of gaseous phase and nanoparticles produced in ultra-shortpulsed laser ablation of transition metal borides, Appl. Surf. Sci. 257 (2011) 5315–5318, doi:10.1016/j.apsusc.2010.11.183.

[21] A. De Bonis, R. Teghil, A. Santagata, A. Galasso, J.V. Rau, Thin films deposited by femtosecond pulsed laser ablation of tungsten carbide, Appl. Surf. Sci. 258 (2012) 9198–9201, doi:10.1016/j.apsusc.2011.07.077.

[22] A. D.e Bonis, A. Galasso, A. Santagata, R. Teghil, Ultrashort pulsed laser ablation of magnesium diboride: plasma characterization and thin films deposition, J. Nanomater. 2015 (2015) 596328, doi:10.1155/2015/596328.

[23] A.L. Patterson, The Scherrer formula for x-ray particle size determination, Phys. Rev. 56 (1939) 978–982, doi:10.1103/PhysRev.56.978.

[24] P.M. Kumar, S. Badrinarayanan, M. Sastry, Nanocrystalline TiO_2 studied by optical, FTIR and X-ray photoelectron spectroscopy: correlation to presence of surface states, Thin Solid Films 358 (2000) 122–130, doi:10.1016/S0040-6090(99)00722-1.

[25] C.-.N. Huang, J.-.S. Bow, Y. Zheng, S.-.Y. Chen, N.J. Ho, P. Shen, Nonstoichiometric titanium oxides via pulsed laser ablation in water, Nanoscale Res. Lett. 5 (2010) 972–985, doi:10.1007/s11671-010-9591-4.

[26] M. Primet, P. Pichat, M.V. Mathieu, Infrared study of surface of titanium dioxides, J. Phys. Chem. 75 (9) (1970) 1216–1220, doi:10.1021/j100679a007.

[27] A.J. Henegar, T. Gougousi, Stability and surface reactivity of anatase TiO_2 films, ECS J. Solid State Sci. 4 (8) (2015) P298–P304, doi:10.1149/2.0041508jss.

[28] M.M. Mazur, Analysis of the properties of functional titanium dioxide thin films deposited by pulsed DC magnetron sputtering with various O_2:arratios, Opt. Mater. 69 (2017) 96–104, doi:10.1016/j.optmat.2017.04.021.

[29] J. Zhang, M. Li, Z. Feng, J. Chen, C. Li, UV Raman spectroscopic study on TiO2. I. Phase transformation at the surface and in the Bulk, J. Phys. Chem. B 110 (2006) 927–935, doi:10.1021/jp0552473.

[30] A.A. Gribb, J.F. Banfield, Particle size effects on transformation kinetics and phase stability in nanocrystalline TiO_2, Am. Mineral. 82 (1997) 717–728, doi:10.2138/am-1997-7-809.

[31] H. Zhang, J.F. Banfield, Understanding polymorphic phase transformation behavior during growth of nanocrystalline aggregates: insights from TiO_2, J. Phys. Chem. B 104 (2000) 3481–3487, doi:10.1021/jp000499j.

[32] V.N. Koparde, P.T. Cummings, Phase transformations during sintering of titania nanoparticles, ACS Nano 2 (2008) 1620–1624, doi:10.1021/nn800092m.

[33] A.J. Bard, L.R. Faulkner, Electrochemical Methods: Fundamentals and Applications, 2nd ed., John Wiley & Sons, 2001.

[34] M. Wagemaker, D. Lützenkirchen-Hecht, A.A. van Well, R. Frahm, Atomic and electronic bulk versus surface structure: lithium intercalation in anatase TiO_2, J. Phys. Chem. B 10 (2004) 12456–12464, doi:10.1021/jp048567f.

[35] M. Wagemaker, R. van de Krol, A.P.M. Kentgens, A.A. van Well, F.M. Mulder, Two phase morphology limits lithium diffusion in TiO_2 (Anatase):a ^7Li MAS NMR study, J. Am. Chem. Soc. 123 (2001) 11454–11461, doi:10.1021/ja0161148.

[36] Z.W. Fu, Q.Z. Qin, Lithium ion diffusion behaviour in laser-deposited TiO_2 films, J. Phys. Chem. B 104 (2000) 5505–5510, doi:10.1021/jp994323x.

[37] H. Lindström, S. Södergen, A. Solbrand, H. Rensmo, J. Hjelm, A. Hagfeldt, S.E. Lindquist, Li+ ion insertion in TiO_2 (anatase). 2. Voltammetry on nanoporous films, J. Phys. Chem. B 101 (1997) 7717–7722, doi:10.1021/jp9639399.

[38] V. Gentili, L.J.Hardwick S.Brutti, A.R. Armstrong, S. Panero, P.G. Bruce, Lithium insertion into anatase nanotubes, Chem. Mater 24 (2012) 4468–4476, doi:10.1021/cm302912f.

[39] W. Ren, M. Qin, Z. Zhu, M. Yan, Q. Li, L. Zhang, D. Liu, L. Mai, Activation of sodium storage sites in Prussian blue analogues via surface etching, Nano Lett. 17 (2017) 4713–4718, doi:10.1021/acs.nanolett.7b01366.

[40] M. Qin, W. Ren, X.Wang J.Meng, X. Yao, Y. Ke, Q. Li, L. Mai, Realizing superior prussian blue positive electrode for potassium storage via ultrathin nanosheet assembly, ACS Sustainable Chem. Eng. 7 (2019) 11564–11570, doi:10.1021/acssuschemeng.9b01454.